

PIV applied to a moving rowing blade

Ernst Jan Grift, Mark Tummers, Edwin Overmars, Jerry Westerweel*

Laboratory for Aero & Hydrodynamics, Delft University of Technology, The Netherlands
*j.westerweel@tudelft.nl

Abstract

We investigate the fluid motion generated by a moving rowing blade. The blade follows a complex path with rather strong acceleration and subsequent deceleration. The blade path is mimicked at a 1:2 scale in a large open-top water tank using a robot system. The tank is transparent, thus enabling full optical access for performing large-field particle image velocimetry (PIV). The robot system allows us to precisely repeat subsequent rowing blade motions. PIV measurements in the same plane show that the fluid motion is highly repeatable, except for the small-scale turbulent fluid motions. When combined with direct measurements of the forces on the rowing blade (Grift et al. 2019a) the PIV data provide insight in the variation of the hydrodynamic forces acting on the blade during motion. This makes it possible to improve the efficiency and effectiveness of the propulsion which is of great relevance to competitive rowing.

Introduction

Competitive rowing is an Olympic sport where the time difference between the winner and the runner up are often very small, usually less than 1 s over a 2,000 m race while a race typically lasts 6 minutes. To increase rowing performance the hydrodynamic propulsion must be optimised, and since race times are so close, small improvements can have a large impact on the outcome of the race. Optimising the propulsion requires better understanding of the motion of the oar blade and the flow field around the oar blade with its corresponding hydrodynamic forces.

The hydrodynamics of a steady flow over an oar blade have been investigated numerically and experimentally, e.g. by Caplan & Gardner (2007) and Coppel et al. (2010), but they neither account for the presence of a free surface, nor do they account for the accelerations and decelerations of the oar blade, or the strong curvature in the blade path. In the works of Sliasis & Tullis (2009), Leroyer et al. (2010) and Robert et al. (2014) the unsteady motion of the oar blade was incorporated in their numerical simulations. They all found that the results for unsteady flow differed substantially from that for steady flow over an oar blade. In the work by Robert et al. (2014) the results are benchmarked against unsteady experimental work by Barré & Kobus (2010) and were found to match reasonably well and only when the free surface and unsteady motion of the oar blade were incorporated. The reasons why the numerical study of the flow around a rowing oar blade is difficult are the high Reynolds number, $10^5 < Re < 10^6$, the presence of a free surface, and the unsteady nature of the flow. Experimental work in a laboratory environment is also difficult because the oar blade path is complex and difficult to replicate, mainly due to the large accelerations and decelerations.

The objective of this study is to provide insights in the flow around a rowing oar blade that can be used to improve rowing performance. To achieve this objective the flow field around a realistic oar blade and for realistic rowing motion is visualised through large-field particle image velocimetry (PIV). With force measurements performed simultaneously to the PIV, the mechanisms that generate propulsion during the drive phase can be identified.

Experimental set-up

Robot and water tank

The experimental set-up used in this study is sketched in figure 1. It is essentially the same set-up as the one described by Grift et al. (2019b) with some minor adaptations. The oar blade motion is reproduced using a 1:2 scale oar blade model attached to a force/torque transducer which, in turn, is mounted on the robot arm of an industrial robot (Reis Robotics RL50) via a cylindrical strut piercing the free surface such that the top of the oar blade coincides with the free surface when it is unperturbed. The robot position is sampled at a default rate of 92 Hz with a resolution of 1 μm and is repeatable within 0.1 mm, which is small with respect to the typical dimensions of the oar blade and its trajectory. The robot arm is placed over an open-top glass tank with a horizontal cross-section of 2 m \times 2 m and a height of 0.6 m, filled with water up to 0.5 m to avoid spilling. The environment and the water in the tank are kept at a temperature of 20°C, to keep the water density and dynamic viscosity constant at $\rho = 1.0 \times 10^3 \text{ kg/m}^3$ and $\mu = 1.0 \times 10^{-3} \text{ Pa s}$, respectively.

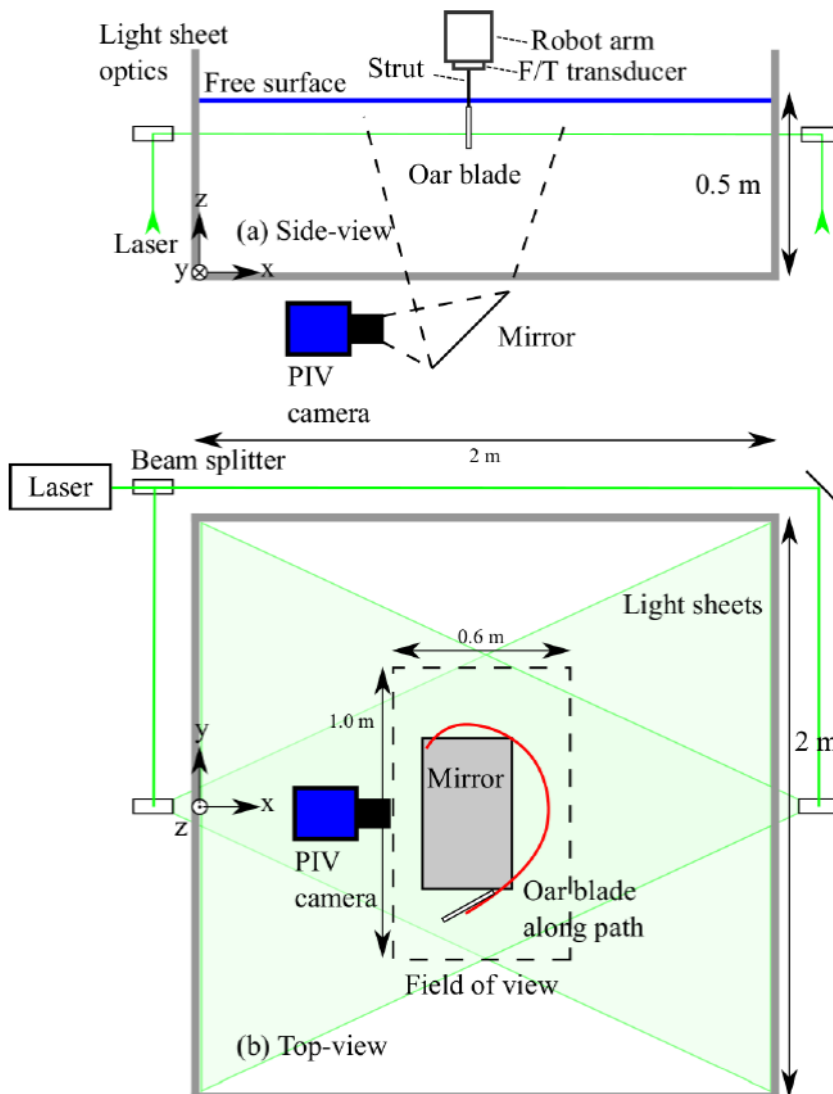


Figure 1: (top) Experimental set-up with the robot holding the oar blade just below the free surface. (bottom) The PIV camera is underneath the tank and captures the oar blade path via a mirror at a 45° angle. Light sheets from opposite sides illuminate the field of view.

PIV system

The vorticity in a selected horizontal plane is obtained through particle image velocimetry (PIV). The plane is chosen at the centre of the blade as indicated in figure 1(top). The tank provides full optical access, i.e. the walls and bottom of the tank are all made of transparent glass. Underneath the tank a PIV camera (Phantom VEO 640L) taking images with 2560×1600 pixels at 500 fps, is positioned parallel to the water surface via a mirror at a 45° angle. The field of view is $0.6 \text{ m} \times 1.0 \text{ m}$. Neutrally buoyant fluorescent spherical tracer particles (10 g Cospheric UVPMS-BR-0.995, $53\text{-}63\mu\text{m}$ diameter) are added to the fluid and are illuminated using two overlapping light sheets from opposing sides to avoid shadows from the opaque oar blade model that is positioned in the light sheet. The light sheets are generated using a single dual cavity Nd:YAG laser beam (Litron 150 W LDY303-HE PIV) followed by a beam splitter.

The acquired images are processed using commercial software (LaVision DaVis 8.4). To create image pairs from the sequential images every frame (n) is paired with the next frame ($n+1$). A multi-pass correlation based PIV algorithm is used to obtain the flow velocity from the image pairs. The interrogation windows used to obtain the velocity fields from the image pairs are set at 64×64 pixels for the first pass and at 32×32 pixels for the two subsequent passes. A 50% overlap between adjacent interrogation positions is used. This results in velocity vector fields with a vector spacing of 6.1 mm and a typical cumulative first and second vector choice of $>98\%$ in the part of the flow perturbed by the blade.

Oar blade kinematics

To determine the oar blade kinematics, a rowing boat passing underneath a bridge was filmed from atop of the bridge. The camera (GoPro Hero 5 black) is aimed downwards, perpendicular to the water surface, and images with 1920×1080 pixels are taken at a frame rate of 120 fps. From the captured images, see figure 2, the oar blade kinematics are obtained by tracking markers on the oar using a correlation based algorithm. The markers on the oar also serve as a calibration target to transform the recorded kinematics from the image domain (“pixels”) to the physical domain (“meters”).

The kinematics of the oar blade are determined for a men's coxless four (M4-) at standard pace, i.e. the pace which can be maintained for a long time without the athletes getting exhausted. All athletes are considered experienced elite rowers.

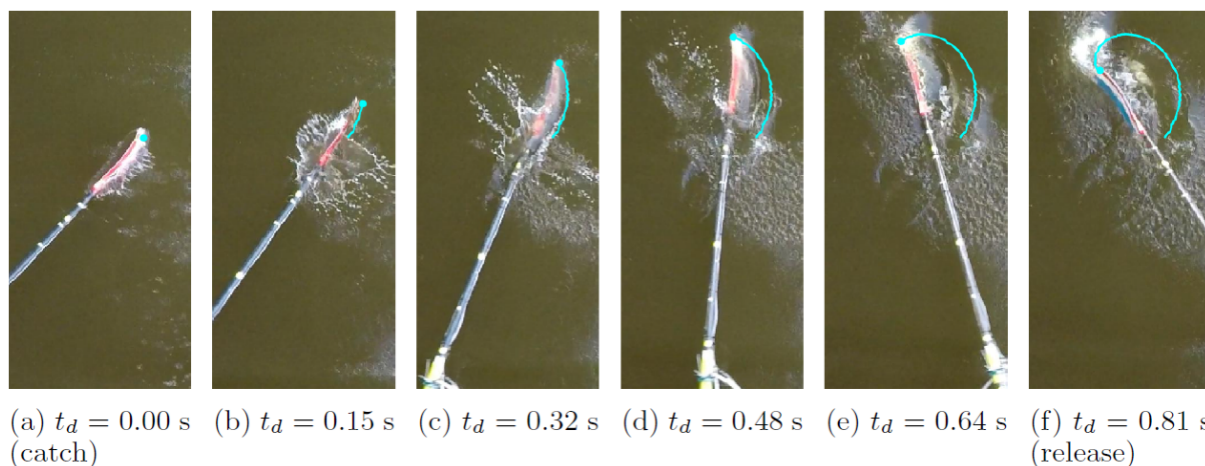


Figure 2: The path of the oar blade tip (solid blue) during the driving phase of a stroke of a men's coxless four (M4-) from catch to release at equidistant moments in time.

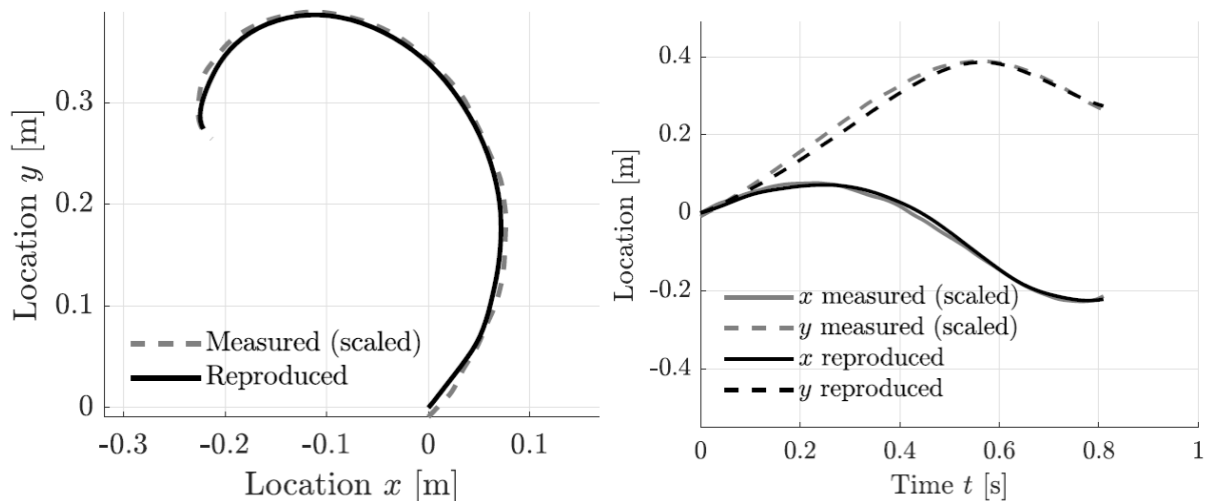


Figure 3: The oar blade tip recorded during on-water rowing scaled with a factor of 2 is represented by the grey dashed line. The black solid line represents the path produced by the robot in the experimental set-up.

Figure 3 shows a comparison between the 1:2 scaled version of the measured path of the oar blade tip and the path reproduced by the robot in the laboratory. The reproduction of the path involves reproducing the geometry, i.e. the path shape, and following the path correctly in time. The path is reproduced very well geometrically as shown in figure 3(left) with maximum deviations of approximately 1 cm. Also, the blade tip coordinates x and y as function of time t are very well reproduced as shown in figure 3(right).

Flow field around the oar blade

To investigate what flow phenomena govern propulsion in rowing we obtain the flow field in a horizontal plane at blade half-height by the use of PIV. The PIV measurements appeared to be highly repeatable (except for the small-scale turbulent fluid motions), so to reduce the noise each measurement is performed three times and is then phase averaged. The z -component of the vorticity ω_z is calculated from the velocity vectors by an 8-point estimation based on the local flow circulation as described by Luff et al. (1999). A characteristic vorticity field is shown in figure 4. In this figure the velocity vectors are also shown to illustrate the resolution of the PIV measurement. In the remainder of this paper the velocity vectors will be shown at a lower density, i.e. some velocity vectors may be skipped, to improve the readability of the figures.

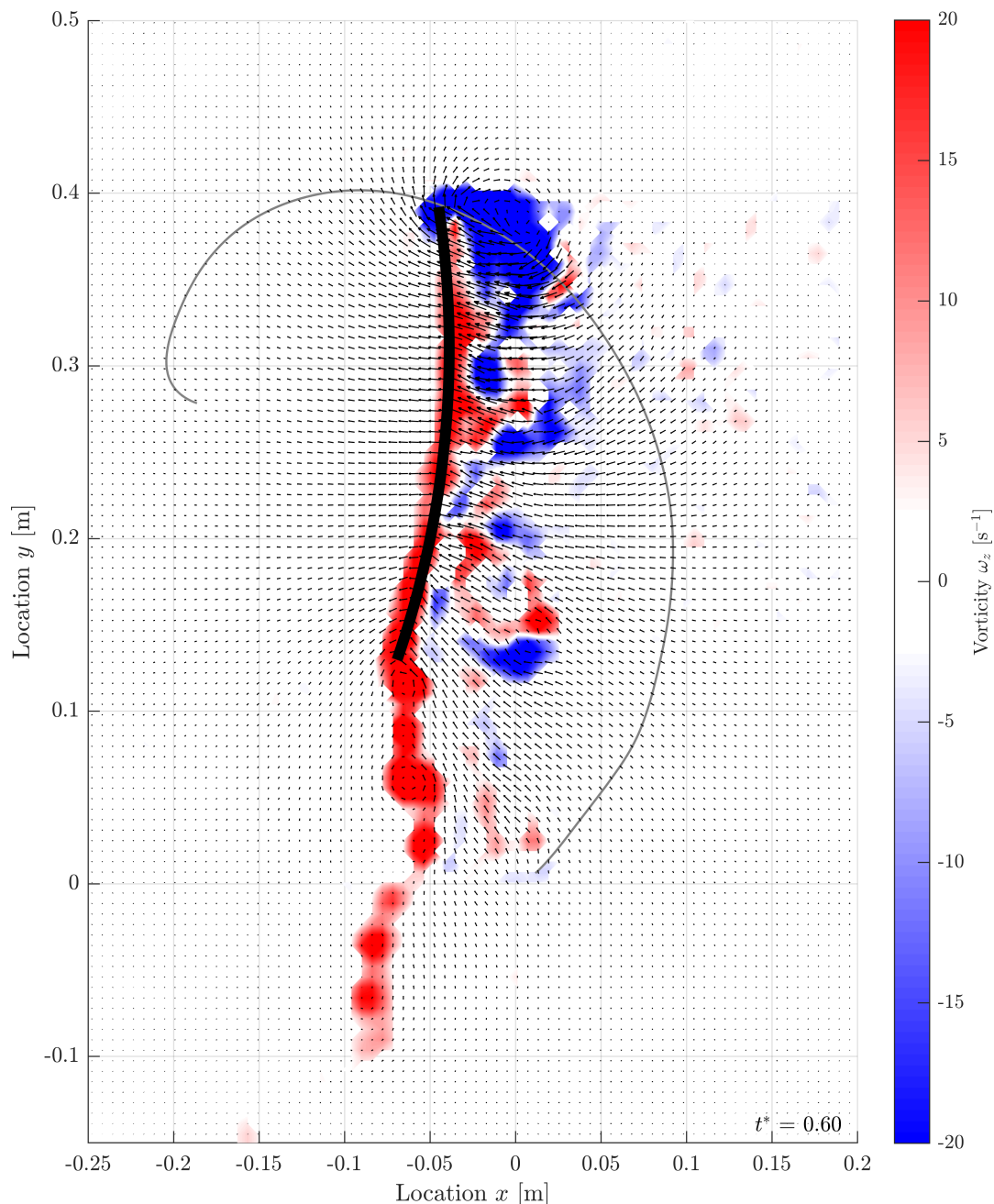


Figure 4: Snapshot of the velocity and vorticity fields. Red and blue colours indicate positive and negative vorticity, respectively. The velocity vectors are shown as black arrows. The oar blade is represented by the thick black line and the oar blade path is shown as a thin grey line.

Figure 5 shows the evolution of the flow field around the oar blade through snapshots for different values of dimensionless time t^* defined as $t^* = (t - t_{\text{catch}}) / (t_{\text{release}} - t_{\text{catch}})$. The drive phase starts at the catch at $t^* = 0$ and location $x = 0, y = 0$. At the start of the drive phase the blade moves away from the boat in positive y -direction and generates lift which contributes to propulsion, i.e. the lift vector has a component in positive x -direction. At $t^* = 0.33$, the blade is in the middle of its lift generation phase. The corresponding flow field is shown in figure 5a. It is clear that a leading edge vortex (LEV) (I) is formed and that a vorticity sheet is attached to the trailing edge of the blade (II). The geometry of the oar blade during this stage is similar to that of a slender airfoil or a curved plate at a small angle of attack. Since the oar blade is rapidly accelerated, its motion could be considered as impulsively started. Indeed, for an impulsively started airfoil a similar vortex sheet at the trailing edge is observed.

Wagner (1925) reported that for an impulsively started airfoil at a small angle of attack, a vortex sheet is formed at the trailing edge and that the lift during the initial translation is small compared to the steady state lift. Only after the airfoil travelled seven chord lengths the lift has reached 90% of its steady state value. The behaviour of the lift during the initial translation follows a curve that is nowadays called the Wagner function. For impulsively started airfoils with a sharp edge, like our oar blade, also an LEV is formed. This LEV can be lift enhancing, when a low pressure zone at the convex side of the blade is formed, or can be detrimental for the generated lift, when the LEV is located at the concave side of the blade or when the LEV moves close to the trailing edge (Li & Wu 2015).

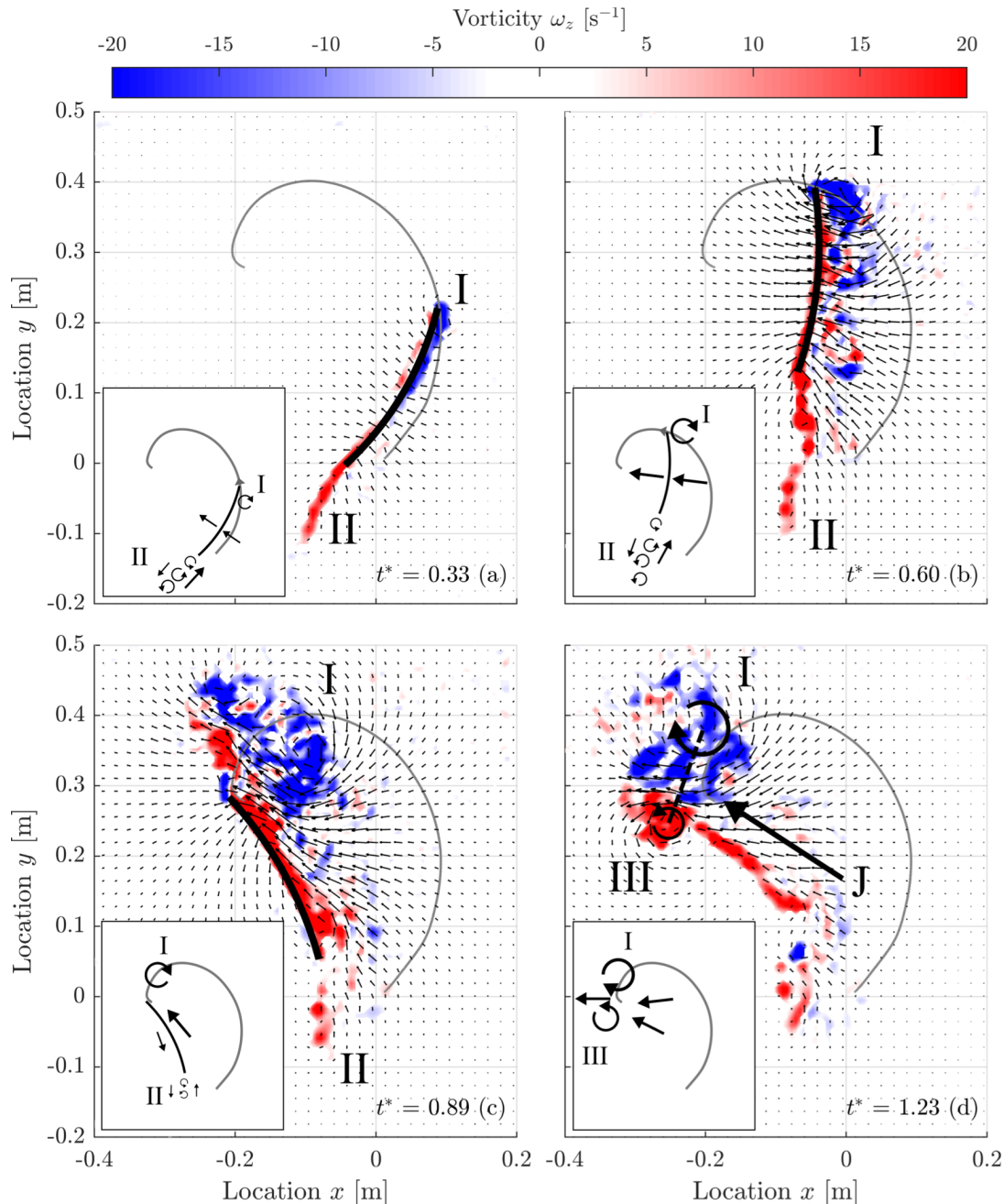


Figure 5: Snapshots of the velocity and vorticity fields taken at (a) the start of the drive phase $t^* = 0.33$, (b) in the middle of the drive phase $t^* = 0.60$, (c) just before the release $t^* = 0.89$ and (d) just after the release $t^* = 1.23$.

In figure 5b the flow field is depicted at time $t^* = 0.60$, where the drag and propulsion are at a maximum. The vortex sheet (II) has grown in length and the leading edge vortex has developed into a larger vortex (I) and has shifted a small distance away from the blade. The angle of attack is now close to 90° (i.e. perpendicular to the path), which explains that drag is at its maximum while lift is close to zero. The large vortex I is still close to the blade and causes a low pressure zone at the convex side of the blade, so it is likely that the presence of the vortex will increase the drag, similar to the trailing vortical structure in the study by Grift et al. (2019b).

In figure 5c the flow field is depicted at time $t^* = 0.89$ where drag is at its minimum and the lift is of opposite sign compared to the lift generated at $t^* = 0.33$, although due to the blade orientation the lift still contributes to propulsion. The trailing vortex (I) has grown even larger in size and the vortex sheet (II) is almost extinct. Although the vortex (I) still exists, it is no longer very close to the blade and its low pressure zone is therefore thought unlikely to cause the measured lift. Instead, we suspect that the velocity difference between both sides of the oar blade causes the observed lift.

In figure 5d the flow field is shown after the release at time $t^* = 1.23$. The large velocity difference between both sides of the oar blade at $t^*=0.89$ developed into a vortex (III) upon the rapid extraction of the oar blade. In combination with the former LEV (I) a vortex pair (I-III) is formed which is also visible at the water surface and will be well known to anyone who has an interest in actual on-water rowing.

Conclusions

An experimental set-up has been built that can be used to study the fluid motion around an oar blade during rowing. With the help of a modified industrial robot a 1:2 scale model of a rowing blade accurately reproduced the complex path of a real rowing blade. A PIV system was used to measure the instantaneous flow and vorticity fields around the blade during the rowing stroke. This gives better insights into the hydrodynamic forces acting on the blade, and may ultimately help to improve rowing performance.

References

- Barré, S. & Kobus, J. M. (2010) Comparison between common models of forces on oar blades and forces measured by towing tank tests. Proceedings of the Institution of Mechanical Engineers, Part P: Journal of Sports Engineering and Technology 224 (1), 37-50.
- Caplan, N. & Gardner, T.N. (2007) A fluid dynamic investigation of the Big Blade and Macon oar blade designs in rowing propulsion. Journal of Sports Sciences 25 (6), 643-650.
- Coppel, A., Gardner, T.N., Caplan, N. & Hargreaves, D. M. (2010) Simulating the fluid dynamic behaviour of oar blades in competition rowing. Proceedings of the Institution of Mechanical Engineers, Part P: Journal of Sports Engineering and Technology 224 (1), 25-35.
- Grift E.J., Tummers M.J. and Westerweel J. (2019a) Hydrodynamics of rowing, J. Fluid Mech. (in preparation).
- Grift E.J., Vijayaragavan N.B., Tummers M.J. and Westerweel J. (2019b) Drag force on an accelerating submerged plate, J. Fluid Mech., Vol. 866, pp. 369-398.
- Leroyer, A., Barré, S., Kobus, J. M. & Visonneau, M. (2010) Influence of free surface, unsteadiness and viscous effects on oar blade hydrodynamic loads. Journal of Sports Sciences 28 (12), 1287-1298.
- Li, J. & Wu, Z.-N. (2015) Unsteady lift for the Wagner problem in the presence of additional leading/trailing edge vortices. J. Fluid Mech., Vol. 769, pp. 182-217.

Luff, J. D., Drouillard, T., Rompage, A. M., Linne, M. A. & Hertzberg, J. R. (1999) Experimental uncertainties associated with particle image velocimetry (PIV) based vorticity algorithms. *Experiments in Fluids* 26 (1-2), pp. 36-54.

Robert, Y., Leroyer, A., Barré, S., Rongère, F., Queutey, P. & Visonneau, M. (2014) Fluid Mechanics in Rowing: The Case of the Flow Around the Blades. *Procedia Engineering* 72, 744-749.

Sliasis, A. & Tullis, S. (2009) Numerical modelling of rowing blade hydrodynamics. *Sports Engineering* 12 (1), 31.

Wagner, H. (1925) Über die Entstehung des dynamischen Auftriebes von Tragflügeln. *ZAMM - Journal of Applied Mathematics and Mechanics / Zeitschrift für Angewandte Mathematik und Mechanik* 5 (1), pp. 17-35.